IMPROVING THE MODELLING OF SURFACE CONVECTION DURING NATURAL NIGHT VENTILATION IN BUILDING ENERGY SIMULATION MODELS

Sarah Leenknegt[1], Rolf Wagemakers[2], Walter Bosschaerts[2], Dirk Saelens[1]
[1]Building Physics Section, K.U.Leuven, Leuven, Belgium
[2]Department of Mechanics, Royal Military Academy, Brussels, Belgium

ABSTRACT

The performance of night ventilation to cool buildings is highly sensitive to the convective surface heat flux. As a result, simulations in BES-models may largely over- or underestimate the real cooling potential of this technique. To assess this, a series of transient 2D CFD-simulations, including thermal mass in floor and ceiling, are made with variation on ACH, inlet temperature and inlet location. It is shown that the location of the inlet strongly influences the surface averaged convective surface heat transfer coefficients at the ceiling. The prediction of the transition from forced to natural convection is important. It is shown that the dimensionless Richardson number at the inlet could be a good indicator.

INTRODUCTION

Night ventilation is a passive method to cool a building. During day, the thermal inertia inside is used to buffer the heat. During night, high air change rates (typically 4 to 10 h^{-1}) are used to cool down the exposed surfaces. Driving forces can be natural or mechanical. Among other parameters, the convective cooling of the surfaces greatly influences the efficiency of night ventilation. The convective heat flux is expressed by Eq. (1), where h_c is the convective heat transfer coefficient (CHTC), T_s is the surface temperature and T_{ref} is a chosen reference temperature.

$$q_c = h_c \cdot (T_s - T_{ref}) \qquad (1)$$

In literature, the sensitivity of night ventilation with regard to the CHTC is already addressed. Breesch & Janssens (2010) investigated natural night ventilation and distinguished between buoyant and stratified horizontal surfaces with different correlations for natural convection. For a temperature difference ΔT between surface and air from 0.1 to 4 K , this resulted in CHTC's for buoyant and stratified horizontal surfaces respectively from 0.71 to 3.59 W/(m².K) and from 0.16 to 0.85 W/(m².K). Also Artmann et al (2008) performed a sensitivity study with regard to night ventilation and found a high sensitivity for the CHTC for values lower than 4 W/(m².K) and for buildings with average mass, which is defined as a building with exposed concrete ceilings and gypsum walls. This is the expected range during night ventilation in real applications.

Though different researchers show that night ventilation can be an efficient cooling technique, its cooling potential is difficult to predict accurately (Breesch, 2006) and is often predicted using Building Energy Simulation (BES) models, such as TRNSYS, Energy+, etc. However, there are still many improvements to be made in the modelling of surface convection in BES-models, especially compared to the state of modelling of radiation and conduction (Goldstein & Novoselac, 2010; Peeters et al, 2011). Common BES-models still assume isothermal surfaces and surface-averaged CHTC. Additionally, only one temperature node is used to describe the room air, assuming perfectly mixed air. Therefore, the selection of an appropriate reference temperature for Eq. (1) is very important. Apart from the simplified modelling of surface convection, a second problem is the selection of an appropriate (surface-averaged) CHTC-value. According to the overview made by Crawley et al (2008), most BES-models allow users to calculate the internal surface convection coefficients depending on temperature differences, hereby putting the emphasis on the use of natural convection correlations. Most BES-tools do allow the user to input their own constants or correlations. However, most users do not have sufficient background to do this accurately or ignore the flow characteristics. As an improvement, some tools offer a coupling between BES and CFD, for example TAS, ESP-r and TRNSYS give this option. As this still requires high computation time as well as high user skills (Peeters et al, 2011) a more pragmatic way is needed. Some tools allow a determination of the CHTC based on the type of air flow. IES<VE>, for example, provides a simplified method, based on the mean room air velocity. However, the most detailed and pragmatic procedure to determine CHTC based on the type of air flow is the correlation selection algorithm developed by Beausoleil-Morrison (2000), which is applied in ESP-r. This selection algorithm distinguishes between five main flow regimes, depending on driving force and cause of temperature differences (Beausoleil-Morrison,

2002). For example: buoyant flow, either caused by surface-to-air temperature differences or by a heating element. The prevailing convection regime for each zone is determined, and a set of appropriate CHTC-equations is selected from a total of 28 equations. Each surface is assigned a correlation, based on its characteristics, for example: vertical wall next to heating element.
Determination of the regime for each zone can be done through a series of user prompts or through the calculation of a dimensionless number. This selection algorithm is also implemented in EnergyPlus, where the Richardson number (Ri) is calculated for each zone. The Ri-number is calculated with Eq. (2), where EnergyPlus utilises the zone height as characteristic length L.

$$Ri = \frac{\beta \cdot g \cdot (T_{warm} - T_{cold}) \cdot L}{u^2} = \frac{Gr}{Re^2} \qquad (2)$$

β is the thermal expansion coefficient of air (K^{-1}), g is the gravity acceleration (m/s²), u is the air velocity (m/s), L is the characteristic length (m), Gr is the Grashof number [-] and Re is the Reynolds number [-].

This pragmatic approach has great merit as it allows a permanent evaluation of the dominant convection regimes throughout the simulation. Also, it is easy to refine further, through the addition of newly developed correlations. In EnergyPlus, new correlations by Fohanno & Polidori (2006) and Goldstein & Novoselac (2010) were added. For night ventilation however, cold air is supplied to a warm room, which may result in large differences between local convection regimes, going from stratified to forced convection. It was shown that it is not straightforward to select an appropriate correlation for floor and ceiling in this case (Leenknegt et al, 2011).

METHODOLOGY

In the current paper, a parameter study was made through unsteady anisothermal 2D-simulations in the CFD-package Fluent 12. The boundary conditions were varied to obtain a variation of the Ri-number between 1 and 10. This should represent mixed to nearly 100% buoyant flow, as the Ri-number gives the ratio of the buoyancy forces to the kinematic forces. Seven cases are simulated, each for two geometries. The boundary conditions for each case are shown in Figure 1. The temperature difference ΔT refers to the difference between initial room air and supply air temperature. The two geometries vary in inlet/outlet location: inlet and outlet are located either directly next to ceiling or at 20 cm distance (Figure 2). The individual cases are denoted consecutively by the ACH, the initial ΔT and the geometry. For example, case 7h2K02 refers to the case with 7 ACH, an initial temperature difference between room air and supply air of 2 K and with inlet and outlet located at 20 cm from the ceiling surface.

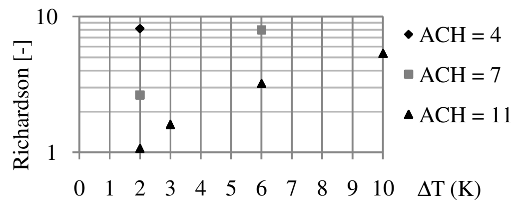

Figure 1 Graphical representation of cases for the parameter variation

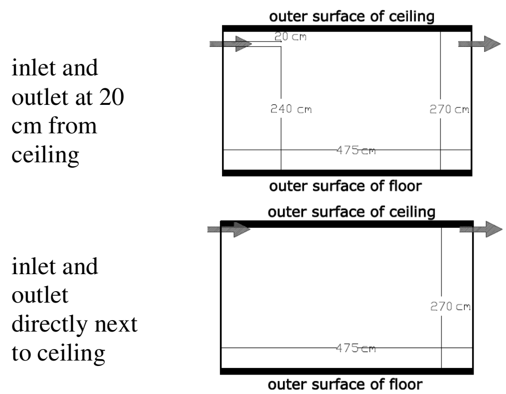

Figure 2 Schematic representation of the simulated office geometries

For these cases it is investigated how the flow pattern evolves over time and how it impacts the local surface convection. The resulting local and surface averaged CHTC's are then compared to existing correlations. Additionally, the transient behaviour is discussed. In order to select appropriate correlations at each time step, an attempt is made to predict the transition between convection regimes.
Finally, a correlation is developed for the CHTC at the ceiling. This correlation was used to estimate the influence of the CHTC at the ceiling on the predicted thermal comfort in TRNSYS. Further information is provided in the next paragraph, which discusses the details of the modelling approach.

MODELLING

A CFD-study is made of the transient conjugate heat transfer between air and thermal mass of the ceiling and floor in a room with high ventilation rate of colder air. The influence of air density variations is taken into account with the incompressible ideal gas law. The simulations are made for a 2D-section of an office. Two geometries with different inlet/outlet location are compared.
As we want to simulate the transient conjugate heat transfer, the internal surfaces cannot be considered as adiabatic, nor can a fixed surface flux be used. Also by imposing a fixed surface temperature, the flux from surface to air is influenced by this boundary condition. Therefore, the choice was made to include solid regions in the mesh to formally include the thermal mass. In office

buildings, the thermal capacity is mainly located in floor and ceiling, as opposed to the light-weight partition walls. Therefore, only the mass in floor and ceiling are taken into account and both vertical walls are considered as adiabatic. The thermal mass consists of 100 mm of heavy reinforced concrete with a density of 2400 kg/m³, capacity of 840 J/(kg.K) and a conductivity of 2.2 W/(m.K). The transient cooling of the air-mass system is simulated for 8 hours.

A sensitivity study was done with regard to turbulence model, near wall treatment and grid sensitivity. A very fine mesh (Figure 3) was generated at the walls and close to the inlet, with y^+-values typically below 1. In order to accurately model the heat transfer through the boundary layer the enhanced wall treatment has been implemented. For the simulations presented in this paper, the RNG k-ε turbulence model was used. According to the review by Zhai et al. (2007) and Zhang et al. (2007), this RANS model is stable and performs well in varying situations (natural and forced convection flows). Susin et al (2009) also describes good results for this model.

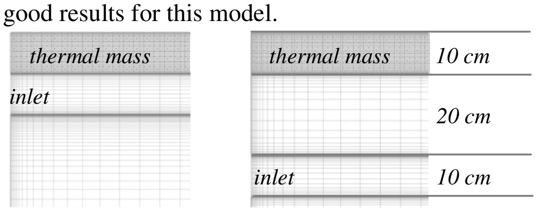

Figure 3 Detail of mesh for two geometries

First an isothermal steady state simulation is made to obtain initial flow conditions. The office is assumed to be at 22 °C, which is considered a representative temperature at the end of the working day in summer. The air change rate is 0.9 h^{-1}, representing the hygienic air change rate during office hours. With this as initial condition, a transient simulation is started with a higher air change rate, representing the increased air change rate during night ventilation. The inlet is modelled as a velocity-inlet, while the outlet is chosen as a pressure-outlet (0 Pa) on the opposite side of the room. Both are located either directly next to the ceiling or at 20 cm from the ceiling with an opening height of 10 cm. The two outer surfaces of the concrete slabs (see Figure 2) are thermally coupled in the CFD-model, as such representing a concrete slab with an equivalent thickness of 20 cm, which is exposed to cold air on both sides.

A variation was made with regard to air change rate, initial temperature difference between inlet and room air and distance from inlet to ceiling. The different cases are given in Table 1, sorted by descending Ri-number, and with dimensionless numbers Grashof (Gr), Reynolds (Re) and Rayleigh (Ra) calculated with following equations:

$$Gr = \frac{\beta \cdot g \cdot (T_{warm} - T_{cold}) \cdot L^3}{\nu^2} \quad (3)$$

$$Re = \frac{u \cdot L}{\nu} \quad (4)$$

$$Ra = \frac{Gr \cdot \nu}{\alpha} \quad (5)$$

β is the thermal expansion coefficient of air (1/K), g is the gravity acceleration (m/s²), u is the inlet air velocity (m/s), L is the characteristic length (m), ν is the kinematic viscosity of air (m²/s) and α is the thermal diffusivity of air (m²/s).

It can be discussed which characteristic length L is an appropriate choice for the calculation of the dimensionless numbers. In a similar study conducted by Sinha (2001) and Tripathi & Moulic (2007), L was chosen as the inlet height. As the buoyancy depends strongly on the height of the thermal gradient, it was considered more appropriate to take L as the height of the room, as was done for the calculation of the Ri-number in Figure 1 and is also done in EnergyPlus. However, to allow easy comparison between different literature sources, the dimensionless numbers in Table 1 are calculated for both definitions of L.

In the study conducted by Sinha (2001) and Tripathi & Moulic (2007), the CFD-simulations were made with a laminar flow model. For natural or forced convection flows, it is determined with respectively the Rayleigh and the Reynolds number whether the flow is turbulent. As we have mixed to natural convection, we look primarily at Ra to evaluate this. For flow over a vertical surface, transition occurs around Ra > 10^8 (ASHRAE, 2001), therefore, the values in Table 1 suggest that the flow in these cases is at least mildly turbulent and a turbulence model should be used when solving the flow.

Table 1 Overview of parameter study: initial conditions and initial dimensionless numbers

case		initial conditions				Grashof		Reynolds		Rayleigh	Richardson	
h^{-1}	ΔT	v_{in}	T_{in}	T_{mass}	T_{air}	L_{inl}	L_{vert}	L_{inl}	L_{vert}	L_{vert}	L_{inl}	L_{vert}
4	2	0.14	20	22	22	$2.9\ 10^5$	$4.3\ 10^9$	$9.43\ 10^2$	$2.31\ 10^4$	$2.10\ 10^9$	0.33	8.12
7	6	0.25	16	22	22	$8.8\ 10^5$	$1.3\ 10^{10}$	$1.65\ 10^3$	$4.04\ 10^4$	$6.29\ 10^9$	0.32	7.95
11	10	0.39	16	22	26	$1.5\ 10^6$	$2.2\ 10^{10}$	$2.59\ 10^3$	$6.35\ 10^4$	$1.05\ 10^{10}$	0.22	5.37
11	6	0.39	16	22	22	$8.8\ 10^5$	$1.3\ 10^{10}$	$2.59\ 10^3$	$6.35\ 10^4$	$6.29\ 10^9$	0.13	3.22
7	2	0.25	20	22	22	$2.9\ 10^5$	$4.3\ 10^9$	$1.65\ 10^3$	$4.04\ 10^4$	$2.10\ 10^9$	0.11	2.65
11	3	0.39	19	22	22	$4.4\ 10^5$	$6.5\ 10^9$	$2.59\ 10^3$	$6.35\ 10^4$	$3.15\ 10^9$	0.07	1.61
11	2	0.39	20	22	22	$2.9\ 10^5$	$4.3\ 10^9$	$2.59\ 10^3$	$6.35\ 10^4$	$2.10\ 10^9$	0.04	1.07

Legend: ΔT (K) the initial temperature difference between the average room air and the supply air; v_{in} (m/s) the inlet velocity; T_{in}, T_{mass} and T_{air} (°C) respectively the initial temperatures of the inlet air, thermal mass and room air; L_{inl} and L_{vert} respectively the height of the inlet and the height of the room as characteristic length for the calculation of *Gr*, *Re*, *Ra* and *Ri*

FLOW PATTERN AND LOCAL CHTC

As the flow pattern will strongly determine the local surface convection coefficients, it is important to visualise the flow and evaluate it parallel with the local convection coefficients. The flow pattern in the room for the different cases can be subdivided in four general flow types. They are shortly discussed here, together with the resulting local CHTC's. Flow type 1 is dominated by buoyancy and occurs at rather high Ri-numbers. It is visualized in Figure 4. The incoming air falls down almost immediately after entering. The air adheres strongly to the flat vertical wall under the inlet and continues over the floor towards the back side of the office. An increase of CHTC occurs at the left side of the floor, where the flow attaches to the surface. At the other side of the room, the air is pulled up towards the outlet, resulting in another increase of the CHTC just after the detachment point. Part of the air flowing upwards leaves the zone through the outlet; the remaining flow hits the ceiling, detaches again and falls down in a wide counter-clockwise vortex in the middle of the room. When the inlet and outlet are located next to the surface, the air velocities next to the surface are much higher; this causes a very high flux just next to the openings. A third peak is then observed just before the main vortex detaches from the ceiling. In case of the lower inlet and outlet, the influence of the openings is still visible though less pronounced. As the air below the remainder of the ceiling surface is strongly stratified, the CHTC stays nearly constant over the length of the room. This is not the case at the floor, where buoyancy is much stronger showing a downward slope making the transition from the left peak to the right peak.

Only for Ri-numbers lower than 1 this flow pattern changes. This is flow type 2 and is visualized in Figure 5. It can be seen here that the incoming air is no longer pulled straight down and either adheres to the ceiling or becomes a free horizontal jet, though only for a short distance, i.e. about 0.5 m. A Coanda-effect, where the flow adheres to a nearby surface, is seen on the vertical wall under the inlet, which is an important factor in the duration of this phase. It must be noted that the geometry here is very simple. In reality, more details would be present here, like a window ledge. This could influence the strength of the Coanda-effect on this surface.

Over the course of time, the incoming jet will slowly penetrate further into the room, creating a small clockwise vortex just under the inlet. The CHTC-profiles on floor and ceiling are very similar to the first phase, though the peaks at the floor become a little smoother and the influence of the protruding jet is seen as a locally higher heat flux at the left side of the ceiling.

It can take hours before the air detaches from the vertical wall. When this happens however, a relatively fast transition flow occurs. The clockwise vortex becomes bigger and the vortex core travels through the room in a matter of 10 to 30 minutes. This is flow type 3 and is illustrated in Figure 6.

Finally, in Figure 7, the flow is no longer buoyancy dominated and a strong Coanda-effect shapes the flow field at the ceiling. The CHTC-profile at the floor is now inversed, with a higher peak at the right and an upwards slope towards the right. At the ceiling, a large peak of the local CHTC is seen at inlet and outlet. Over the remaining ceiling surface the CHTC is also higher due to the forced flow here, though the CHTC decreased strongly over the length of the ceiling until it reaches the second peak at the outlet.

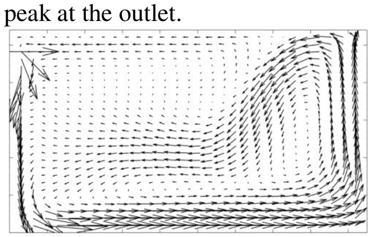

Figure 4 Flow type 1 - buoyancy dominant

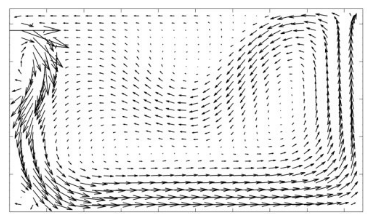

Figure 5 Flow type 2 – Coanda on vertical wall

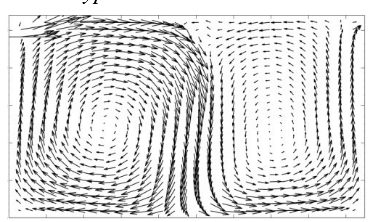

Figure 6 Flow type 3 – fast transition regime

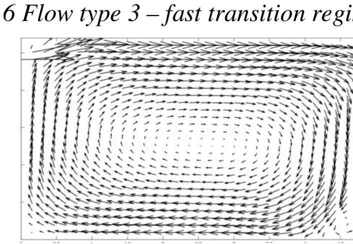

Figure 7 Flow type 4 - forced flow

When the flow pattern in the room is known, the global convection regime at each surface can be estimated. Nevertheless, extreme local values can have a large impact on the surface-averaged value, causing higher CHTC's than expected based on the flow classification. This is discussed in the following paragraph.

LOCAL SURFACE CONVECTION

Correlations from literature usually give equations to calculate the surface averaged CHTC for a given convection regime and surface orientation. They are composed to represent a surface-averaged value. Many correlations are still based on measurements on isolated flat plates. Their values can therefore be used to evaluate local convection regimes as well. Comparing them with the local CHTC-values resulting from the CFD-simulations is a way to verify the simulation and understand the local convection regimes. This is done for the simulated cases.

For the floor, and throughout all simulated cases, the surface averaged CHTC lies within the range of 1.2 to 2.4 W/(m².K), without taking the initial 15 minutes into account. This is shown on Figure 8. These values were compared with existing correlations from literature, locally at discrete times and averaged over the surface throughout the simulated flow time. Due to the large local differences near the attachment and detachment points no good local fit with existing correlations could be obtained. However, based on the surface averaged values, two main correlations came forward. For flows with initial high Ri-number during flow types 1 and 2, the CHTC's at the floor correspond reasonably well with the forced convection correlation for wall-sided diffusers from Fisher (1995). These values are situated around 2-2.25 W/(m².K). When the initial Ri-number is lower, a better correspondence is seen with the natural convection correlation from Alamdari & Hammond (1983) for a buoyant floor, with values situated around 1.2-1.6 W/(m².K). It would seem more likely that these two correlations were exchanged. However, the differences between two compared correlations for the same convection regime were in the same order of magnitude as the differences between two similar cases. It is therefore difficult to draw conclusions from this comparison. During flow type 4, there is again good correspondence with the natural convection correlation for a buoyant floor from Alamdari & Hammond (1983).

At the ceiling, the full range of observed averaged CHTC-values varies from 0.3 to 3.3 W/(m².K), without taking the initial 15 minutes into account. This is shown on Figure 9. This is a much wider range than for the floor. The possible sensitivity is therefore higher. A second remark with regard to the ceiling CHTC's is that there is a clear influence of the geometry, which was not at all the case for the floor. For flow types 1 and 2, the main portion of the flow adjacent to the ceiling surface is strongly stratified. For the cases with inlet/outlet not adjacent to the ceiling, this is reflected in the surface-averaged values as well and the influence of the openings on the surface averaged value is negligible. However, when inlet/outlet are located adjacent to the ceiling, the surface-averaged values are always higher. This is due to the local increased fluxes next to the openings, which cause a much higher surface averaged CHTC than expected. For example for case 7h2K00 during flow type 1, the best match is found for a buoyant flow over a horizontal surface by Alamdari & Hammond (1983), though the flow adjacent to the main part of the surface is strongly stratified.

After transition into flow type 4, a clear correspondence is seen with the forced convection correlation from Fisher for wall-sided ceiling diffusers (1995). However, the influence of inlet/outlet location remains valid, as can be seen on Figure 9. It can be concluded that even when the dominant convection regime is correctly identified at a given surface, the influence of the geometry must be taken in to account.

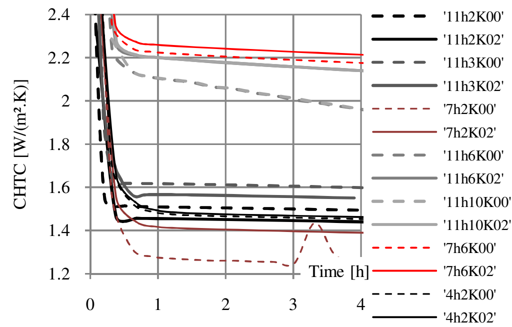

Figure 8 Surface averaged CHTC at floor

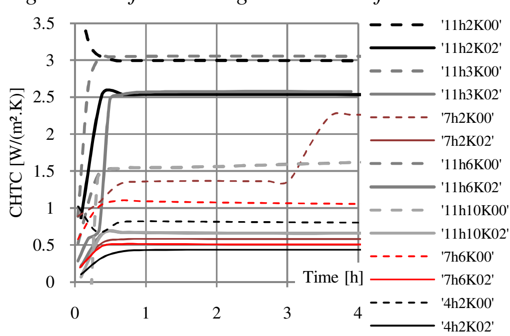

Figure 9 Surface averaged CHTC at ceiling

TRANSIENT BEHAVIOUR

It is shortly summarized here how the flows evolve over time for the different simulated case. In Figure 10 the cases are sorted in descending initial Ri-number at inlet. The cases with higher initial Ri-number continue to have a strong Coanda-effect on the vertical wall during the full simulation time of 8 hours. This is the case for 4 h^{-1} with ΔT of 2 K and 7 h^{-1} with ΔT of 6 K. When the ACH is increased to 11 h^{-1} at ΔT of 6 K or 10 K, the air detaches partly from the vertical wall, starting flow type 2, and progresses very slowly into the room. A full transition is however never reached for these cases, regardless of inlet/outlet location. Only in the three remaining cases, a transition into flow type 4 is observed.

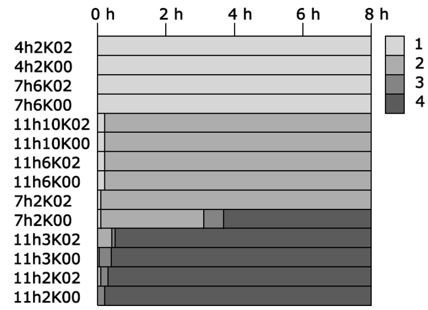

Figure 10 Timing of flow transition for all cases

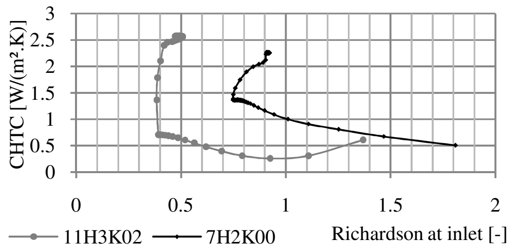

Figure 11 Surface averaged CHTC at the ceiling in function of the Richardson number at the inlet

With the transition into forced flow, an important increase of the convective heat flux at the ceiling is observed. The CHTC will be much higher than is expected by natural convection correlations. Therefore, with regard to BES-models, it is very important to be able to predict when this transition will occur. This was investigated for the simulated cases. When the inlet is located next to the ceiling, it occurs around Ri-values of 0.75-0.8. From this point, the kinetic forces are not only strong enough to prevent the air from falling down, but also to create a Coanda-effect at the ceiling to counter the Coanda at the wall underneath the inlet. Indeed, when the inlet is located lower, the transition occurs only at Ri-number around 0.4. A near-isothermal situation is required before a sufficiently strong Coanda-effect is realised at the ceiling. This is illustrated for case 7h2K00 and 11h3K02 in Figure 11. A sharp increase in CHTC at the ceiling is seen during the transition.

The transient behaviour can be discussed in more detail for the case 7h2K00, as three different flow patterns are observed here. The surface averaged CHTC on floor and ceiling, as well as Ri-number at the inlet are displayed on Figure 12(a). The Ri-number is calculated with T_{warm} from Eq. (2) taken as the room averaged air temperature, as the room air is very well mixed. Initially, a very fast decline of the Ri-number can be seen, corresponding with a fast mixing of the incoming air with the room air and therefore fast decrease in room average air temperature. After the initial mixing period, a slow further decline can be seen over the next 2.5-3 hours. A large change can be seen around 3 h of flow time. A fast increase of the CHTC at the ceiling indicates that the flow pattern is changing from a flow dominated by buoyancy (flow type 2) into a forced convection flow (flow type 4).

In parallel, the CHTC at the floor varies due to the change in the flow pattern. After stabilization of the flow, the CHTC stabilizes as well, at a similar value as before. Finally, the Ri-number increases as well during the transition phase, which is due to the higher heat flux from the ceiling, resulting in a slight increase of the room averaged air temperature, visible on Figure 12(b).

After stabilization of the flow, CHTC-values remain constant and a slow further decrease of the Ri-number and surface and air temperature is seen.

IMPLEMENTATION IN BES-MODEL

As demonstrated above, it is shown that the dominant flow type can be predicted with the Ri-number at the inlet. Therefore, an attempt is made to find a general correlation between the surface-averaged CHTC at the ceiling and this Ri-number at the inlet. For each simulated case, the Ri-number at the inlet and the surface averaged CHTC a point were calculated for every few minutes of flow time. The result is shown in Figure 13, where two plots are made for the two geometries. An exponential function is fitted through the data points. A reasonable fit is achieved with inlet/outlet adjacent to ceiling (CL_CHTC_case00) and is summarized in Eq. (6).

$$h = 10{,}3 \cdot \left[\frac{\mathrm{u_{sup}}^2}{\mathrm{L} \cdot (\mathrm{T_a} - \mathrm{T_{sup}})}\right]^{0.55} \tag{6}$$

L is the room height (m), T_a and T_{sup} are respectively the average room air and the supply air temperature (K) and u_{sup} is the supply air velocity (m/s).

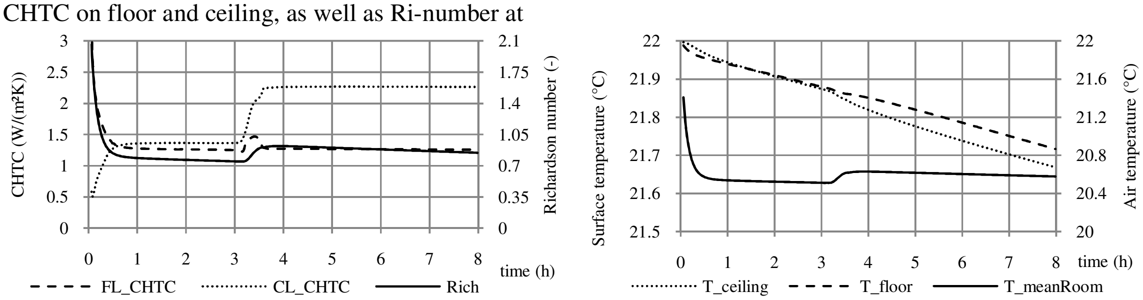

a. Richardson and surface averaged CHTC

b. Surface and room averaged air temperature

Figure 12 Time evolution of thermal parameters for 7 h^{-1}, ΔT of 2 K and inlet at 20 cm from ceiling

It must be noted that this equation has by no means the ambition to be generally valid, as it is only based on 2D-simulations for a simplified geometry. It does not take into account the surface temperature, so is only valid for building elements with similar thermal diffusity and with a positive surface to air temperature difference. It can however be used to quantify the sensitivity of the thermal comfort after night ventilation for the simulated cases in BES. This is done in the next paragraph.

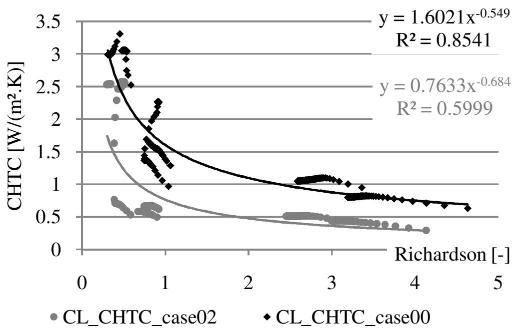

Figure 13 CHTC at ceiling in function of the Ri-number at inlet

In the dynamic energy simulation program TRNSYS the thermal response of a similar geometry has been simulated for 6 of the different boundary condition sets (case 11h10K was omitted as it is quasi identical to 11h6K). A schedule is used for the boundary conditions as given in Table 2, temperatures are initialized at 22 °C. The simulation was run for 1 day, and the results of this day are compared with regard to surface and air temperatures. The limit air temperature is taken at T_{lim} = 23 °C and the weighted overheating hours WOH are calculated as in Eq. (7). The resulting WOH are given in Table 3.

$$WOH = \sum_{i=8-9h}^{17-18h} max[T_{a,i} - T_{lim}, 0] \qquad (7)$$

We see that the influence of the new correlation (V1) is limited when compared to the internal calculation (%_V2). However, when compared to the simulation with fixed CHTC (%_V3), the influence is very high. The internal calculation overestimates the overheating slightly for the cases where forced convection occurs (11h2K, 11h3K). The CHTC at the ceiling is underestimated slightly here. For the other cases, the natural convection correlations from the internal calculation in TRNSYS perform quite well, as this is indeed the dominant flow. The difference with the simulation with fixed CHTC is much higher, as the CHTC is continuously higher than for either of the other two versions. The buffering capacity during the day is therefore much higher than when the natural convection correlations are used, which results in much lower overheating hours.

Table 2 – Boundary conditions TRNSYS

<table>
<tr><th>time</th><th>version 1</th><th>version 2</th><th>version 3</th></tr>
<tr><td rowspan="2">0h-8h</td><td colspan="3">high ventilation flow with low supply air temperature, in accordance with each case, no internal gains</td></tr>
<tr><td>Eq. (6) for CHTC at ceiling</td><td>internal calculation of CHTC by TRNSYS</td><td rowspan="2">fixed value of 3 W/(m².K) at ceiling, recommended by TRNSYS</td></tr>
<tr><td rowspan="2">8h-24h</td><td colspan="2">internal calculation of CHTC</td></tr>
<tr><td colspan="3">hygiënic ventilation flow of 1 ACH at 18 °C</td></tr>
<tr><td>8h30-18h30</td><td colspan="3">constant internal gains present, 24 W/m², 100 % convective, 0 % radiative</td></tr>
</table>

Table 3 – Resulting WOH on the first day

WOH	11h 2K	11h 3K	7h 2K	11h 6K	7h 6K	4h 2K
V1	26.3	25.0	27.2	20.8	22.8	28.0
V2	27.2	25.7	27.5	20.9	22.2	27.9
V3	19.1	17.4	19.7	12.1	13.8	20.4
%_V2	**-3.2**	**-3.0**	**-1.0**	**-0.3**	**2.7**	**0.1**
%_V3	**27.4**	**30.4**	**27.8**	**41.6**	**39.6**	**27.2**

%_Vx gives the relative difference between Vx en V1, with V1 as reference.

CONCLUSIONS

14 transient 2D CFD simulations were made, with variation of ACH, inlet temperature and location of inlet and outlet. The mass was included in the model in order to monitor the transient convective cooling of the floor and ceiling slab. It was investigated how the modelling of surface convection can be improved in BES-models for such cases. It is shown that the selection of an appropriate correlation for the situation of cold air supplied to a room remains a problem. We see a few reasons for this:

Some BES-models, like TRNSYS, focus only on natural convection correlations for the automatic calculation of CHTC's. For nearly isothermal rooms and/or very high air supplies, the convection can be much higher, especially on surfaces close to the inlet. No standard mixed or forced convection correlations are provided. This is different when a correlation selection algorithm is implemented. This leads however to a second problem, being the prediction of the transition of the local flow from natural towards mixed and forced convection.

The dimensionless Richardson number can be used to predict this transition, as it gives the ratio of the buoyancy forces over the kinematic forces. The characteristic length was taken as the height of the room. The location of the inlet (distance to the ceiling) is of great importance. For an inlet located next to the ceiling, the transition occurs around Ri-values of 0.75-0.8, while for inlets located 20 cm lower, a value of only 0.4 is more appropriate. The Coanda-effect on the wall underneath the inlet can delay the transition for hours. However, after a critical Ri-value is reached, the transition occurs relatively fast, i.e. within 10 to 30 minutes. It must be noted that these values were found for a simplified geometry with a flat vertical surface under the inlet. The presence of window ledges etc. was not taken into account.

The accurate prediction of the occurrence of forced convection is very important. The range of values in surface-averaged CHTC at the ceiling varied from 0.3 to 3.3 W/(m².K), which is a much wider range than was found for the CHTC on the floor. For example, in EnergyPlus, when a horizontal free jet is present in the zone, it is assumed that the Coanda-effect will occur, and the correlations for ceiling diffusers are used instead of the correlations for a horizontal free jet (Fisher, 1995). However, the simulations made for this research strongly suggest that only for nearly isothermal rooms or very high inlet air velocities, this assumption can be made. Even then are the correlations for a horizontal free jet likely much higher than for a stratified ceiling. This assumption could therefore result in a large overestimation of the convective surface heat flux at the ceiling.

Finally, a correlation was developed for the ceiling, as a function of the Ri-number, based on the CFD-results. This correlation was used in TRNSYS and the resulting thermal comfort was compared for this correlation, the internal calculation of TRNSYS and a fixed value. The internal calculation gave an overestimation of the overheating hours by 3% for the forced flow cases, which is still rather good. All the simulations with fixed value gave a large underestimation of the overheating, as the suggested value is too high.

ACKNOWLEDGEMENTS

This research was funded by the Research Foundation Flanders (FWO Vlaanderen). Their financial contribution is greatly appreciated.

REFERENCES

Alamdari, F., Hammond, G.P., (1983) Improved data correlations for buoyancy-driven convection in rooms, Building Services Engineering Research & Technology 4, p. 106-112

Artmann et al, (2008) Parameter study on performance of building cooling by night-time ventilation, Renewable Energy 33, p. 2589-2598

ASHRAE Handbook of Fundamentels, (2001)

Beausoleil-Morrison, I., (2000) PhD. The adaptive coupling of heat and air flow modeling within dynamic whole-building simulation, University of Strathclyde, Glasgow, UK

Beausoleil-Morrison, I., (2002) The adaptive simulation of convective heat transfer at internal building surfaces, Building and Environment 37, p. 791-806

Breesch, H., (2006) PhD. Natural night ventilation in office buildings. Performance evaluation based on simulation, uncertainty and sensitivity analysis, UGent, Belgium

Breesch, H., Janssens, A., (2010) Performance evaluation of passive cooling in office buildings based on uncertainty and sensitivity analysis, Solar Energy 84, p. 1453-1467

Crawley et al, (2008) Contrasting the capabilities of building energy performance simulation programs, Building and Environment 43, p. 661-673

Fisher, D.E., (1995) PhD. An experimental investigation of mixed convection heat transfer in a rectangular enclosure, University of Illinois, Urbana, USA

Fohanno, S., Polidori, G., (2006) Modelling of natural convective heat transfer at an internal surface, Energy and Buildings 38, p. 548-553

Goldstein, K., Novoselac, A., (2010) Convective heat transfer in rooms with ceiling slot diffusers, HVAC&R Research 16(5), p. 629-655

Leenknegt et al, (2011) Towards a more reliable modelling of night-time ventilation with Building Energy Simulation models, Proceedings of Roomvent 2011, Trondheim, Norway

Peeters et al, (2011) Internal convective heat transfer modelling: Critical review and discussion of experimentally derived correlations, Energy & Buildings 43, p. 2227-2239

Sinha, S.L., (2001) Behaviour of inclined jet on room cooling, Building & Environment 36, p. 569-578

Susin et al., (2009) Evaluating the influence of the width of inlet slot on the prediction of indoor air flow: Comparison with experimental data, Building and Environment 44, 971-986

Tripathi, B, Moulic, S.G., (2007) Investigation of the buoyancy affected airflow patterns in the enclosure subjected at the different wall temperatures, Energy & Buildings 39, p. 906-912

Zhai et al., (2007) Evaluation of Various Turbulence Models in Predicting Airflow and Turbulence in Enclosed Environments by CFD - Part-1: Summary of Prevalent Turbulence Models, HVAC&R Research 13(6), 853-870

Zhang et al., (2007) Evaluation of various turbulence models in predicting airflow and turbulence in enclosed environments by CFD: Part 2 – comparison with experimental data from literature, HVAC&R Research, 13(6), ASHRAE, 871-886